Supporting Information for Role of Base Strength, Cluster Structure and Charge in Sulfuric Acid-Driven Particle Formation

Nanna Myllys,[*,†,‡,‖] Jakub Kubečka,[‡] Vitus Besel,[‡] Dina Alfaouri,[‡] Tinja Olenius,[¶] James Smith,[†] and Monica Passananti[§,‡]

†*Department of Chemistry, University of California, Irvine*

‡*Institute for Atmospheric and Earth System Research, University of Helsinki*

¶*Department of Environmental Science and Analytical Chemistry & Bolin Centre for Climate Research, Stockholm University*

§*Dipartimento di Chimica, Universitá di Torino*

‖*+358 503812141*

E-mail: nanna.myllys@uci.edu

Cluster Structures and Gibbs Free Binding Energies

As stated in the main text, we have used cluster structures of our previous works as a base of our study.[1–3] For cluster structures not studied before, we have performed a new configurational sampling procedure, explained below. In addition, if some previously found cluster structures seemed to be outlying from the general trends, we have re-sampled them to find a better configuration.

First, we used a recently introduced genetic algorithm, the Artificial Bee Colony (ABC) algorithm,[4] to explore the Potential Energy Surface (PES) of the desired molecular cluster. We utilized the ABCluster program,[5,6] which uses ABC to explore the PES of clusters composed of rigid molecular units. Assuming rigidity of molecules is no problem since the molecular clusters will be optimized in the further steps. Thus, assuming all possible combinations of molecular units (isomers and protonation states) we explored the PES on the Molecular Mechanics (MM) level with Force Field (FF) parameters taken from the CHARMM database.[7,8] We used the following ABCluster specification: 2000 initial random guesses, 100 generations (exploration loops) and 5 scout bees, and saved 5000 energetically lowest-lying local minima for each combination of molecular units.

Second, all structures found by ABCluster were re-optimized by the tight-binding semi-empirical program GFN-xTB with very tight optimization criteria.[9] Many of the structures relaxed to the same minimum on the PES. Thus, we removed all redundant structures based on the total GFN-xTB energy and the radius of gyration (a geometry property incorporating cluster size and mass distribution). Two structures were combined if the total GFN-xTB energy difference was lower than 0.001 Hartree and the gyration radius difference was lower than 0.01 Ångström. We also removed energetically high-lying local minima, if the relative total GFN-xTB energy with respect to the energetically lowest-lying structure was higher than $5\times N$ kcal/mol, where N is the number of molecules in the cluster.

The next step was optimization at the ωB97X-D/6-31++g** level of theory[10] with very tight optimization criteria. However, not all structures from the GFN-xTB step were used

due to a large amount of minima configurations remaining that fulfilled all above listed conditions. First, we did a uniform sampling/selection of 50 structures based on their GFN-xTB energy and radius of gyration. Second, after optimization of these 50 structures on DFT level of theory, we re-selected another 50 structures from the GFN-xTB step around the structures chosen in the primary selection. This set formed the lowest-lying structures on DFT level of theory. Thus, we selected overall 100 structures after the GFN-xTB step.

Finally, for few energetically lowest-lying cluster structures (0–2N kcal/mol, where N is the number of molecules in the cluster), we performed vibrational frequency analysis to obtain thermal corrections for the free energies. On top of the 2–5 lowest DFT free energy structures, we calculated the single point electronic energy corrections using DLPNO-CCSD(T)/aug-cc-pVTZ level of theory. The DLPNO single point energy and the DFT thermal correction were used to calculate the Gibbs free energy of the cluster. The Gibbs free binding energies for the global minimum energy clusters are calculated as:

$$\Delta G = G_{\text{cluster}} - \sum_i G_{\text{monomers},i}. \tag{1}$$

As mentioned, the Gibbs free binding energy is a sum of the DLPNO binding energy (ΔE) and the DFT thermal contribution ($\Delta G_{\text{Thermal}}$), calculated as

$$\Delta G = \Delta E + \Delta G_{\text{Thermal}}. \tag{2}$$

Table S1 presents ΔE, $\Delta G_{\text{Thermal}}$ and ΔG. The compounds are referred to as follows: A=sulfuric acid, N=ammonia, D=dimethylamine, G=guanidine, B=bisulfate and P=proton. The corresponding cluster structures in xyz format are found in the supplementary zip folder.

Table S1: Binding energies (ΔE, DLPNO), thermal contributions to the Gibbs free energy ($\Delta G_{\text{Thermal}}$, DFT) and Gibbs free binding energies (ΔG, DLPNO//DFT). All values are in kcal/mol, $\Delta G_{\text{Thermal}}$ and ΔG are calculated at 298.15 using RRHO approximation.

Cluster	ΔE	$\Delta G_{\text{Thermal}}$	ΔG
1A1N	-16.433	9.674	-6.759
1A2N	-31.280	19.711	-11.569
1A3N	-43.184	33.445	-9.739
1A4N	-55.680	45.252	-10.427
2A1N	-46.742	25.380	-21.362
2A2N	-66.389	37.463	-28.926
2A3N	-82.373	50.157	-32.216
2A4N	-95.896	61.380	-34.515
3A1N	-67.730	37.106	-30.625
3A2N	-94.650	50.837	-43.813
3A3N	-119.675	63.878	-55.798
3A4N	-139.217	79.208	-60.009
4A1N	-89.101	51.613	-37.488
4A2N	-121.308	67.715	-53.593
4A3N	-147.440	79.872	-67.568
4A4N	-173.116	89.714	-83.402
2N	-3.187	6.934	3.747
3N	-10.703	19.198	8.495
4N	-16.595	29.850	13.254
1B1N	-10.519	11.742	1.224
1B2N	-18.836	20.001	1.165
1A1B1N	-59.246	27.076	-32.170
1A1B2N	-69.183	38.538	-30.645
2A1B1N	-97.249	41.036	-56.213
2A1B2N	-114.240	51.916	-62.324
2A1B3N	-131.945	65.654	-66.325
3A1B1N	-126.408	52.311	-74.098
3A1B2N	-151.355	67.207	-84.148
3A1B3N	-173.355	81.412	-91.942
3A1B4N	-196.468	97.104	-99.232
4A1B1N	-155.362	67.777	-87.585
4A1B2N	-179.504	80.065	-99.439
4A1B3N	-209.649	94.894	-114.756
4A1B4N	-224.474	105.423	-119.051
1P2N	-26.281	7.202	-19.079
1P3N	-46.015	18.098	-27.917
1P4N	-60.051	21.935	-32.830
1P5N	-75.667	34.809	-40.858

1A1P1N	-21.279	5.914	-15.365
1A1P2N	-55.088	19.524	-35.564
1A1P3N	-74.080	30.104	-43.975
1A1P4N	-90.996	39.969	-51.027
1A1P5N	-108.197	51.044	-56.952
2A1P1N	-47.851	20.672	-27.180
2A1P2N	-82.511	33.532	-48.978
2A1P3N	-115.137	47.440	-67.697
2A1P4N	-132.884	56.720	-76.164
2A1P5N	-150.004	65.851	-84.153
3A1P3N	-138.154	59.693	-78.461
3A1P4N	-168.922	73.662	-95.260
3A1P5N	-187.215	85.253	-101.962
4A1P4N	-192.803	86.155	-106.648
4A1P5N	-228.170	101.998	-126.172
1A1D	-24.819	11.284	-13.535
1A2D	-40.462	23.234	-17.227
1A3D	-57.275	36.394	-20.881
1A4D	-71.532	50.226	-21.306
2A1D	-58.921	26.287	-32.634
2A2D	-90.137	41.564	-48.574
2A3D	-111.094	55.169	-55.925
2A4D	-126.846	66.712	-60.134
3A1D	-84.855	40.667	-44.188
3A2D	-120.432	55.775	-64.657
3A3D	-154.415	71.166	-83.249
3A4D	-178.359	85.309	-93.051
4A1D	-105.456	54.449	-51.007
4A2D	-144.846	69.843	-75.004
4A3D	-179.242	83.415	-95.827
4A4D	-213.369	97.940	-115.429
2D	-5.042	9.366	4.324
3D	-14.493	20.991	6.498
4D	-23.794	29.633	5.839
1B1D	-13.207	12.991	-0.216
1B2D	-24.328	23.172	-1.156
1A1B1D	-70.197	28.490	-41.707
1A1B2D	-84.320	41.011	-43.309
2A1B1D	-106.951	41.579	-65.371
2A1B2D	-133.061	56.689	-76.372
2A1B3D	-154.180	70.495	-83.686
3A1B1D	-134.801	54.872	-79.929
3A1B2D	-170.166	70.638	-99.528
3A1B3D	-195.297	83.973	-111.324
3A1B4D	-219.245	101.100	-118.145

4A1B1D	-162.690	68.157	-94.534
4A1B2D	-207.598	86.072	-121.527
4A1B3D	-241.279	101.698	-139.580
4A1B4D	-273.940	118.960	-154.980
1P2D	-24.908	9.182	-15.726
1P3D	-44.506	20.311	-24.195
1P4D	-56.313	31.010	-25.304
1P5D	-67.728	44.177	-23.551
1A1P1D	-19.343	8.990	-10.354
1A1P2D	-63.088	22.505	-40.583
1A1P3D	-92.305	37.373	-54.932
1A1P4D	-111.390	49.229	-61.934
1A1P5D	-129.838	61.392	-68.446
2A1P1D	-39.520	21.241	-18.279
2A1P2D	-91.584	35.393	-56.191
2A1P3D	-133.102	50.947	-82.155
2A1P4D	-162.995	65.504	-97.491
2A1P5D	-185.235	79.626	-105.609
3A1P3D	-157.622	65.200	-92.422
3A1P4D	-199.011	80.104	-118.907
3A1P5D	-230.617	97.488	-133.130
4A1P4D	-223.576	93.344	-130.233
4A1P5D	-263.655	107.864	-155.790
1A1G	-30.345	10.044	-20.302
1A2G	-52.747	23.937	-28.809
1A3G	-76.585	38.060	-38.525
1A4G	-97.699	51.765	-45.934
2A1G	-65.589	27.227	-38.362
2A2G	-106.176	37.930	-68.247
2A3G	-129.138	55.360	-73.778
2A4G	-150.019	66.192	-83.826
3A1G	-91.208	39.927	-51.281
3A2G	-138.199	55.189	-83.011
3A3G	-178.926	67.737	-111.189
3A4G	-214.788	81.387	-133.401
4A1G	-113.420	53.471	-59.948
4A2G	-161.413	67.611	-93.802
4A3G	-213.363	82.747	-130.616
4A4G	-269.588	99.840	-169.748
2G	-13.567	11.328	-2.239
3G	-27.759	24.688	-3.071
4G	-49.213	38.883	-10.330

1B1G	-21.563	10.558	-11.231
1B2G	-44.943	27.296	-17.217
1A1B1G	-71.817	21.375	-50.441
1A1B2G	-117.100	42.689	-58.651
2A1B1G	-150.481	56.253	-74.411
2A1B2G	-178.731	69.906	-104.285
2A1B3G	-99.152	40.500	-111.669
3A1B1G	-158.606	54.321	-94.229
3A1B2G	-197.222	73.133	-124.089
3A1B3G	-223.469	85.811	-150.197
3A1B4G	-184.365	72.696	-173.899
4A1B1G	-233.876	83.680	-108.825
4A1B2G	-266.749	97.873	-137.658
4A1B3G	-275.856	101.957	-168.876
4A1B4G	-314.018	113.462	-200.556
1P2G	-28.627	9.909	-18.336
1P3G	-52.232	21.005	-31.227
1P4G	-72.036	31.573	-40.463
1P5G	-88.317	47.432	-40.885
1A1P1G	-19.917	10.449	-9.206
1A1P2G	-69.606	20.300	-49.306
1A1P3G	-103.704	32.990	-70.714
1A1P4G	-120.782	49.165	-71.617
1A1P5G	-148.753	64.248	-84.505
2A1P1G	-41.233	20.834	-19.866
2A1P2G	-93.668	35.120	-58.548
2A1P3G	-144.459	50.910	-93.550
2A1P4G	-180.443	64.274	-116.170
2A1P5G	-206.754	80.566	-126.188
3A1P3G	-169.544	66.634	-102.909
3A1P4G	-221.984	83.139	-138.845
3A1P5G	-258.888	93.617	-165.271
4A1P4G	-251.241	95.151	-156.090
4A1P5G	-293.456	108.633	-184.823
2A	-18.958	11.410	-7.547
3A	-37.797	24.634	-13.163
4A	-56.320	34.358	-21.962
1A1B	-48.364	14.530	-33.834
2A1B	-78.291	27.099	-51.192
3A1B	-105.120	39.503	-65.617
4A1B	-124.215	52.852	-71.363

Evaporation Rates

The evaporation rates of the clusters are obtained from the Gibbs free binding energies ΔG of the evaporating cluster and its products as

$$\gamma_{(i+j)\rightarrow i,j} = \beta_{i,j} \frac{p_{\mathrm{ref}}}{k_{\mathrm{B}} T} \exp\left(\frac{\Delta G_{i+j} - \Delta G_i - \Delta G_j}{k_{\mathrm{B}} T} \right). \tag{3}$$

The collision coefficients for neutral–neutral collisions are computed from kinetic gas theory as

$$\beta_{i,j} = \left(\frac{3}{4\pi} \right)^{1/6} \left[6 k_{\mathrm{B}} T \left(\frac{1}{m_i} + \frac{1}{m_j} \right) \right]^{1/2} \left(V_i^{1/3} + V_j^{1/3} \right)^2, \tag{4}$$

where m_i and V_i are the mass and volume of cluster i, respectively. The volumes are calculated using bulk liquid densities (1830, 696, 680 and 1550 $\frac{kg}{m^3}$ for sulfuric acid, ammonia, dimethylamine and guanidine, respectively) assuming spherical clusters and ideal mixing.

In collisions between ions and neutral molecules or clusters, the collision cross section is larger than that predicted from the physical dimensions of the colliding systems due to their long-range attraction.[11] For the neutral-ion collision coefficients we have applied the approach by Su and Chesnavich,[12] who performed trajectory simulations of collisions between a point charge and a rigidly rotating molecule. The collision frequency is dependent on three reduced parameters:

$$\begin{aligned} \beta_{i,j}^{L} &= q_i \left(\tfrac{1}{m_i} + \tfrac{1}{m_j} \right)^{1/2} \left(\tfrac{\pi \alpha_j}{\epsilon_0} \right)^{1/2} \\ I^* &= \tfrac{\mu_j I}{\alpha_j q_i} \left(\tfrac{1}{m_i} + \tfrac{1}{m_j} \right) \\ x &= \tfrac{\mu_j}{(8\pi\epsilon_0 \alpha_j k_{\mathrm{B}} T)^{1/2}} \end{aligned}$$

where q_i is the charge of the ion, α_j, μ_j, and I are the polarizability, dipole moment, and moment of inertia of the neutral molecule, respectively, and ϵ_0 is the vacuum permittivity. At low values of I^*, *i.e.* when $I^* < \frac{0.7+x^2}{2+0.6x}$, the collision rate was observed to be independent

of I^*, and a fit to the simulated data produced the parametrization

$$\beta_{i,j} = \begin{cases} \beta_{i,j}^{L} \left(0.4767x + 0.6200\right), & x \geq 2 \\ \beta_{i,j}^{L} \left(\frac{(x+0.5090)^2}{10.526} + 0.9754\right), & x < 2. \end{cases} \tag{5}$$

The parametrization has been compared with experimental collision rates and was found to give a good correspondence.[11]

Figure S1 shows the evaporation rates of all studied clusters.

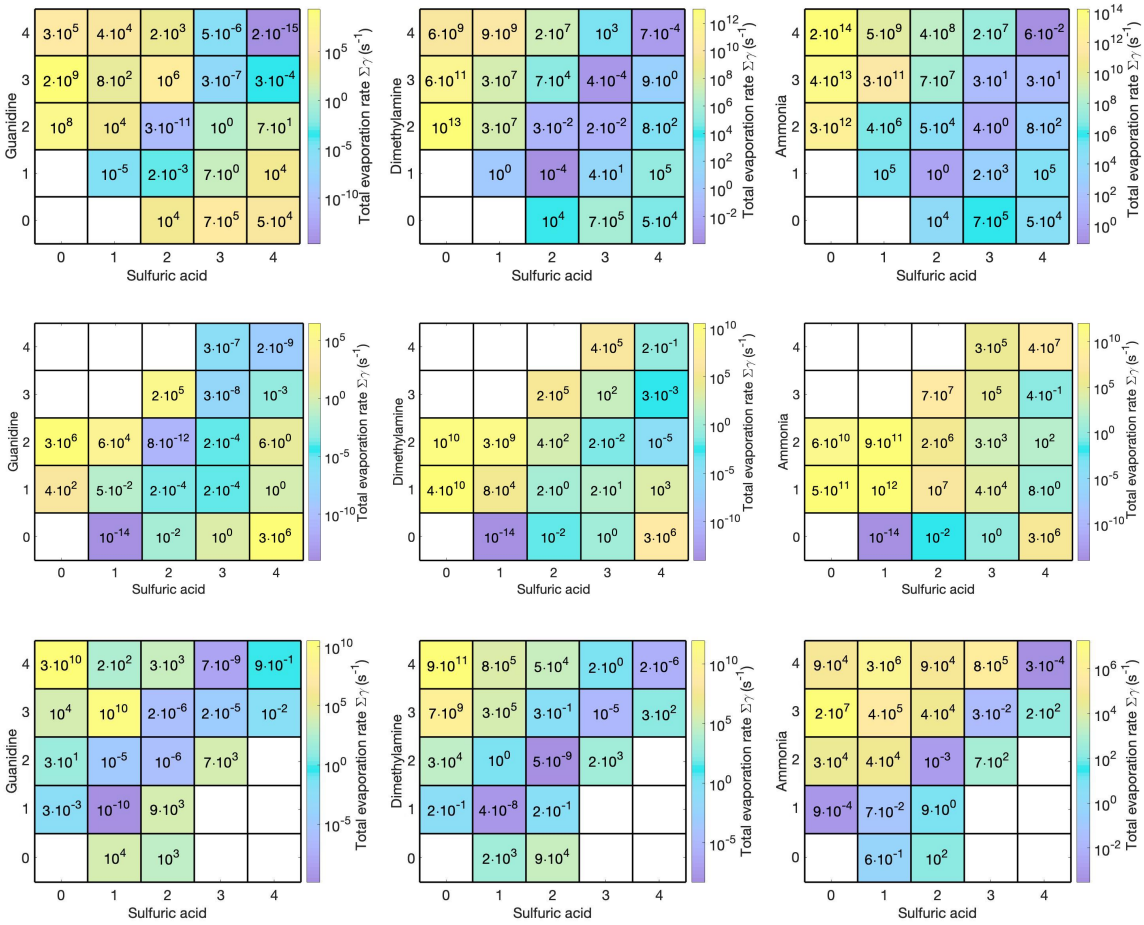

Figure S1: Evaporation rates of sulfuric acid clusters with guanidine (left), dimethylamine (middle) and ammonia (right). First row: neutral clusters, second row: anionic cluster (each cluster contains one bisulfate ion) and third row: cationic clusters (each cluster contains one protonated base).

Cluster Population Dynamics Simulations

The time evolution and behavior of a population of clusters of different sizes and compositions is obtained by integrating the time derivatives of the cluster concentrations using the Atmospheric Cluster Dynamics Code.[13] These birth–death equations include all possible processes where the clusters can be formed or destroyed. For cluster i of a given composition, the time derivative is

$$\begin{aligned}\frac{dC_i}{dt} =& \frac{1}{2}\sum_{j<i}\beta_{j,(i-j)}C_jC_{(i-j)} + \sum_j \gamma_{(i+j)\rightarrow i,j}C_{(i+j)} - \sum_j \beta_{i,j}C_iC_j - \\ & \frac{1}{2}\sum_{j<i}\gamma_{i\rightarrow j,i-j}C_i + S_i - L_iC_i,\end{aligned} \tag{6}$$

where C_i is the concentration of cluster i, $\beta_{i,j}$ is the collision rate coefficient between i and j, $\gamma_{(i+j)\rightarrow i,j}$ is the evaporation rate coefficient of cluster $(i+j)$, S_i is an external source term, and L_i is an external loss term corresponding to coagulation onto pre-existing surfaces. The loss rate L_i was assumed to depend on cluster size according to the parametrization by Lehtinen *et al.*[14] The reference loss rate, corresponding to a sulfuric acid molecule, was set to 10^{-3} s^{-1}, and the scavenging coefficient m to -1.6 corresponding to typical atmospheric conditions. ACDC is available from the authors upon request.

Boundary Conditions

By boundary conditions we refer to the smallest clusters outside of the simulation box which can be assumed to be stable (evaporation rate $\ll 10^{-1}$ s^{-1}). This selection has been done based on the evaporation rates presented in Figure S1. The following boundary conditions are used in the particle formation simulations:

- Neutral sulfuric acid–guanidine: 5A4G and 4A5G
- Anionic sulfuric acid–guanidine: 5A1B4G and 4A1B5G
- Cationic sulfuric acid–guanidine: 5A5G1P and 4A6G1P
- Neutral sulfuric acid–dimethylamine: 5A4D

- Anionic sulfuric acid–dimethylamine: 5A1B4D
- Cationic sulfuric acid–dimethylamine: 4A6D1P
- Neutral sulfuric acid–ammonia: 5A4N
- Anionic sulfuric acid–dimethylamine: 5A1B3N
- Cationic sulfuric acid–dimethylamine: 5A5N1P.

Electrically Neutral Particle Formation

Based on the Gibbs free energies, we simulated new-particle formation rates with the ACDC model and compared the results to atmospheric measurements,[15–17] investigating which simulated base concentrations yield NPF rates close to the measurements. It should be noted that our simulations consider only a single base at a time and the effect of hydration has not been considered, whereas atmospheric measurements include contributions of multiple compounds and synergistic effects might have a significant role. Figure S2 shows the simulated NPF rates considering only electrically neutral molecular clusters for each base, together with the rates deduced from measurements. The figure includes NPF rates at four different base concentrations that yield results close to the experimental rates at atmospherically relevant sulfuric acid vapor concentrations.

In the case of guanidine and sulfuric acid, a guanidine concentration of 0.001–1 $\mathrm{ppt_V}$ is needed to yield NPF rates of the magnitude of the observations. In the sulfuric acid–dimethylamine case, dimethylamine concentration of 0.1–100 $\mathrm{ppt_V}$ is needed, and ammonia-enhanced particle formation requires 10^4–10^7 $\mathrm{ppt_V}$ of ammonia. However, as stated above, these results address two-component systems: it has been demonstrated that the presence of ammonia increases particle formation when added to a two-component sulfuric acid–amine system.[2,18,19] Due to the fact that in the atmosphere ammonia is in practice always present, it can thus be assumed that even lower dimethylamine concentrations can produce NPF rates of the order of the observations.

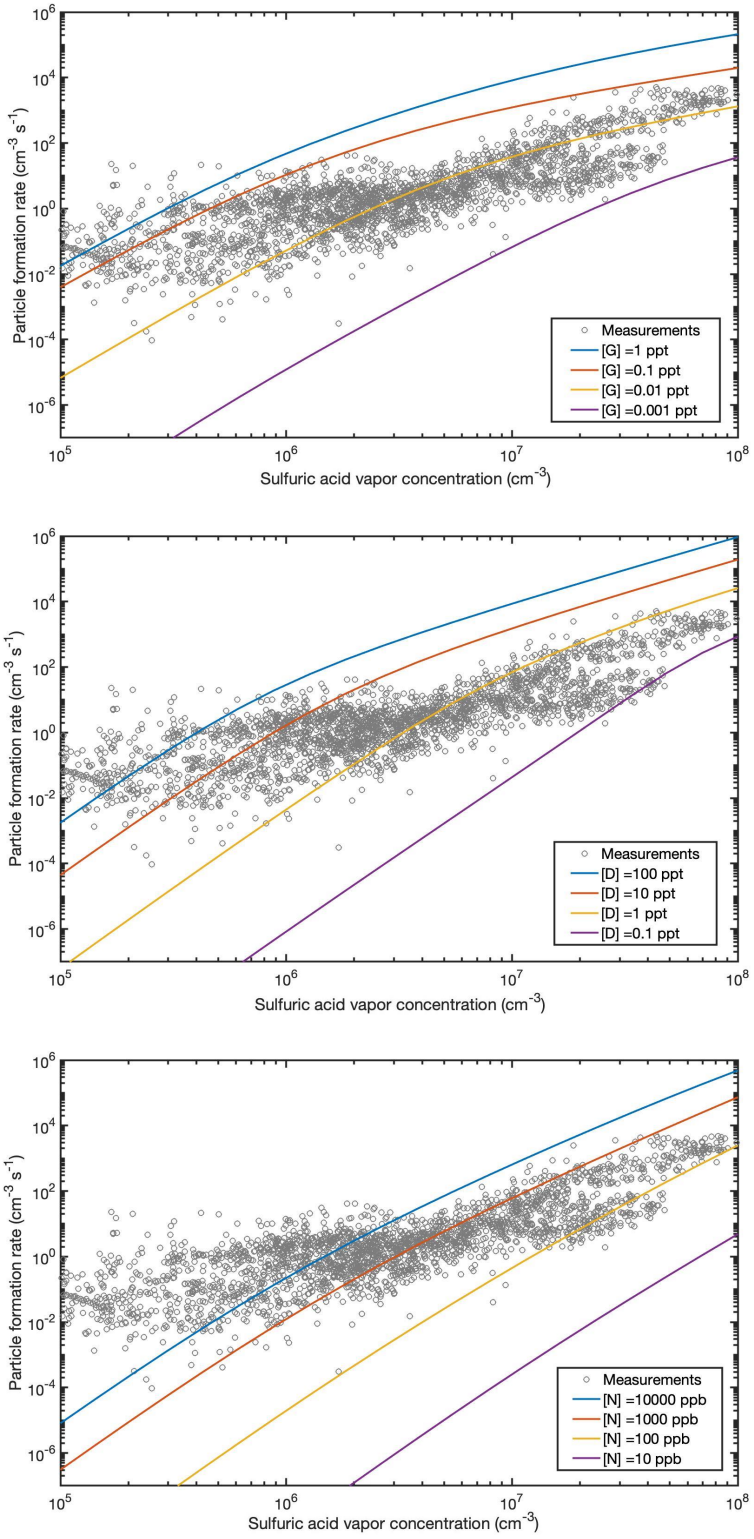

Figure S2: Simulated (lines) and observed (markers) new-particle formation rates as a function of sulfuric acid vapor concentration. Different base concentrations are used for guanidine (top), dimethylamine (middle) and ammonia (bottom).

References

(1) Myllys, N.; Ponkkonen, T.; Passananti, M.; Elm, J.; Vehkamäki, H.; Olenius, T. Guanidine: A Highly Efficient Stabilizer in Atmospheric New-Particle Formation. *J. Phys. Chem. A* **2018**, *122*, 4717–4729.

(2) Myllys, N.; Chee, S.; Olenius, T.; Lawler, M.; Smith, J. N. Molecular-Level Understanding of Synergistic Effects in Sulfuric Acid–Amine–Ammonia Mixed Clusters. *J. Phys. Chem. A* **2019**, *0*, just accepted.

(3) Olenius, T.; Kupiainen-Määttä, O.; Ortega, I. K.; Kurtén, T.; Vehkamäki, H. Free Energy Barrier in the Growth of Sulfuric Acid–Ammonia and Sulfuric Acid–Dimethylamine Clusters. *J. Chem. Phys.* **2013**, *139*, 084312.

(4) Karaboga, D.; Basturk, B. On the Performance of Artificial Bee Colony (ABC) Algorithm. *Appl. Soft Comput.* **2008**, *8*, 687–697.

(5) Zhang, J.; Dolg, M. ABCluster: The Artificial Bee Colony Algorithm for Cluster Global Optimization. *Phys. Chem. Chem. Phys.* **2015**, *17*, 24173–24181.

(6) Zhang, J.; Dolg, M. Global Optimization of Clusters of Rigid Molecules using the Artificial Bee Colony Algorithm. *Phys. Chem. Chem. Phys.* **2016**, *18*, 3003–3010.

(7) Vanommeslaeghe, K.; Hatcher, E.; Acharya, C.; Kundu, S.; Zhong, S.; Shim, J.; Darian, E.; Guvench, O.; Lopes, P.; Vorobyov, I.; Jr., A. D. M. CHARMM General Force Field: A Force Field for Drug-Like Molecules Compatible with the CHARMM All-Atom Additive Biological Force Fields. *J. Comput. Chem.* **2010**, *31*, 671–690.

(8) Yu, W.; He, X.; Vanommeslaeghe, K.; Jr., A. D. M. Extension of the CHARMM General Force Field to Sulfonyl-Containing Compounds and Its Utility in Biomolecular Simulations. *J. Comput. Chem.* **2012**, *33*, 2451–2468.

(9) Grimme, S.; Bannwarth, C.; Shuskov, P. A Robust and Accurate Tight-Binding Quantum Chemical Method for Structures, Vibrational Frequencies, and Noncovalent Interactions of Large Molecular Systems Parametrized for all spd-Block Elements (Z = 1-86). *J. Chem. Theory Comput.* **2017**, *13*, 1989–2009.

(10) Chai, J.-D.; Head-Gordon, M. Long-Range Corrected Hybrid Density Functionals with Damped Atom-Atom Dispersion Corrections. *Phys. Chem. Chem. Phys.* **2008**, *10*, 6615–6620.

(11) Kupiainen-Määttä, O.; Olenius, T.; Kurtén, T.; Vehkamäki, H. CIMS Sulfuric Acid Detection Efficiency Enhanced by Amines Due to Higher Dipole Moments: A Computational Study. *J. Phys. Chem. A* **2013**, *117*, 14109–14119.

(12) Su, T.; Chesnavich, W. J. Parametrization of the Ion–Polar Molecule Collision Rate Constant by Trajectory Calculations. *J. Chem. Phys.* **1982**, *76*, 5183–5185.

(13) McGrath, M. J.; Olenius, T.; Ortega, I. K.; Loukonen, V.; Paasonen, P.; Kurtén, T.; Kulmala, M.; Vehkamäki, H. Atmospheric Cluster Dynamics Code: a Flexible Method for Solution of the Birth–Death Equations. *Atmos. Chem. Phys.* **2012**, *12*, 2345–2355.

(14) Lehtinen, K. E.; Maso, M. D.; Kulmala, M.; Kerminen, V.-M. Estimating Nucleation Rates from Apparent Particle Formation Rates and vice versa: Revised Formulation of the Kerminen–Kulmala Equation. *J. Aerosol Sci.* **2007**, *38*, 988–994.

(15) Paasonen, P. et al. On the Roles of Sulphuric Acid and Low-Volatility Organic Vapours in the Initial Steps of Atmospheric New Particle Formation. *Atmos. Chem. Phys.* **2010**, *10*, 11223–11242.

(16) Sihto, S.-L.; Kulmala, M.; Kerminen, V.-M.; Dal Maso, M.; Petäjä, T.; Riipinen, I.; Korhonen, H.; Arnold, F.; Janson, R.; Boy, M.; Laaksonen, A.; Lehtinen, K. E. J. Atmospheric Sulphuric Acid and Aerosol Formation: Implications from Atmospheric

Measurements for Nucleation and Early Growth Mechanisms. *Atmos. Chem. Phys.* **2006**, *6*, 4079–4091.

(17) Kuang, C.; McMurry, P. H.; McCormick, A. V.; Eisele, F. L. Dependence of Nucleation Rates on Sulfuric Acid Vapor Concentration in Diverse Atmospheric Locations. *J. Geophys. Res. Atmos.* **2008**, *113*.

(18) Yu, H.; McGraw, R.; Lee, S.-H. Effects of Amines on Formation of Sub-3 nm Particles and Their Subsequent Growth. *Geophys. Res. Lett.* **2012**, *39*, 2.

(19) Glasoe, W.; Volz, K.; Panta, B.; Freshour, N.; Bachman, R.; Hanson, D.; McMurry, P.; Jen, C. Sulfuric Acid Nucleation: An Experimental Study of the Effect of Seven Bases. *J. Geophys. Res. Atmos.* **2015**, *120*, 1933–1950.